Electronic Supplementary Material (ESI) for Sustainable Energy & Fuels.

Supporting Information:

Designed synthesis of hierarchical $MoSe_2$@WSe_2 hybrid nanostructure as bifunctional electrocatalyst for total water-splitting

Rajeev Kumar Rai[†], Bidushi Sarkar[†], Ranit Ram[†], Karuna Kar Nanda[†], and N. Ravishankar[*†]

[†]Materials Research Centre, Indian Institute of Science, Bangalore-560012, India

1 Supporting Figures

[*]nravi@iisc.ac.in

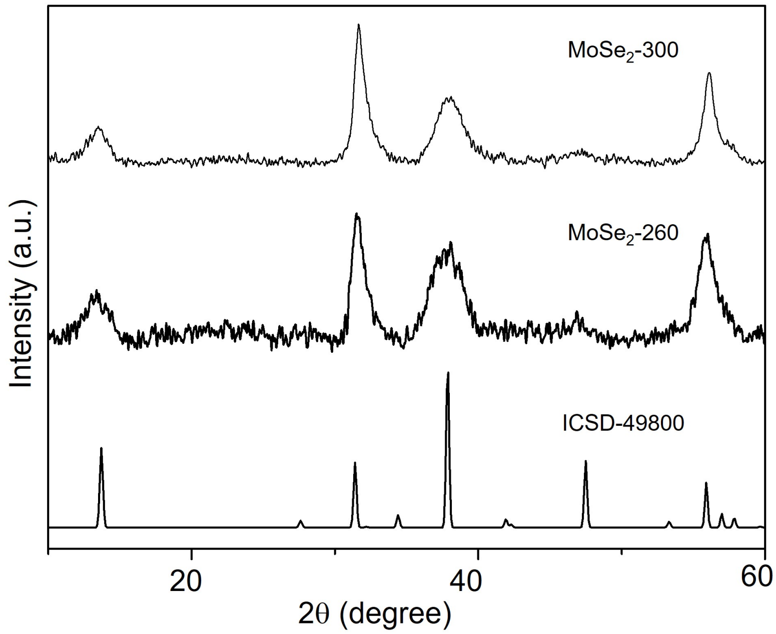

Fig. S1: XRD of $MoSe_2$ synthesized at different temperature. A reference XRD pattern of $MoSe_2$ (ICSD collection code: 49860) is shown in lower panel. Even at low-temperature such as 260 °C, $MoSe_2$ forms as predominant product.

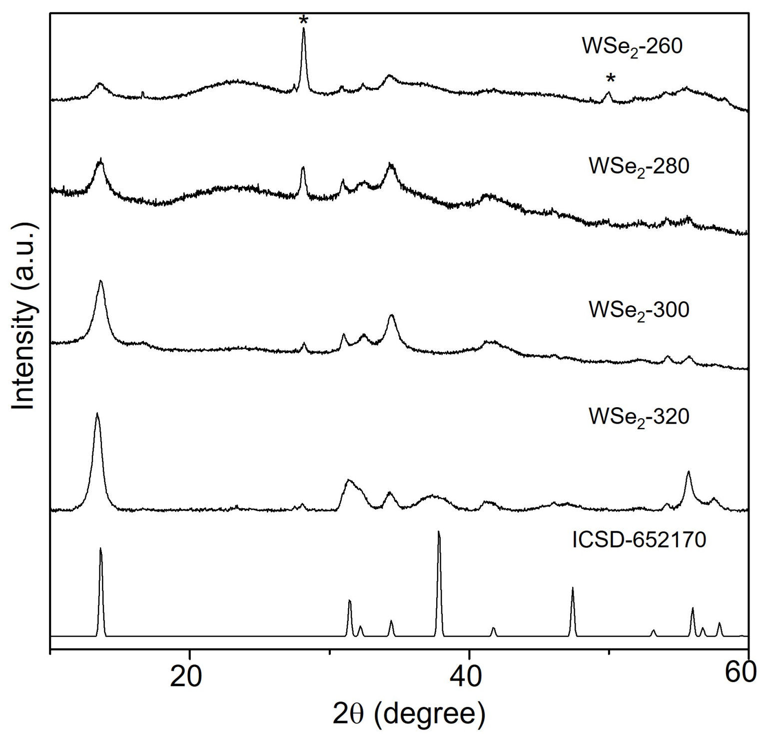

Fig. S2: XRD of WSe_2 synthesized at different temperature, major impurity peaks of WO_3 have been marked with *. A reference XRD pattern of WSe_2 (ICSD collection code: 652170) is shown in lower panel. At low temperature WO_3 is the predominant product, with increase in temperature WSe_2 fraction increases and at 320 °C WSe_2 forms as predominant product.

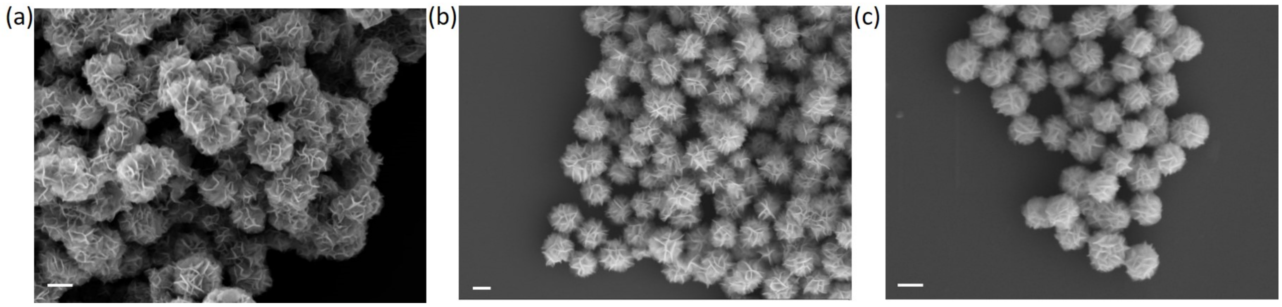

Fig. S3: SEM micrograph of as-synthesized hierarchical nanostructure with different ratio of Mo to W (a) Composition A; (b) Composition B, and (c) Composition C. Scale bar shown in the micrographs represent 200 nm.

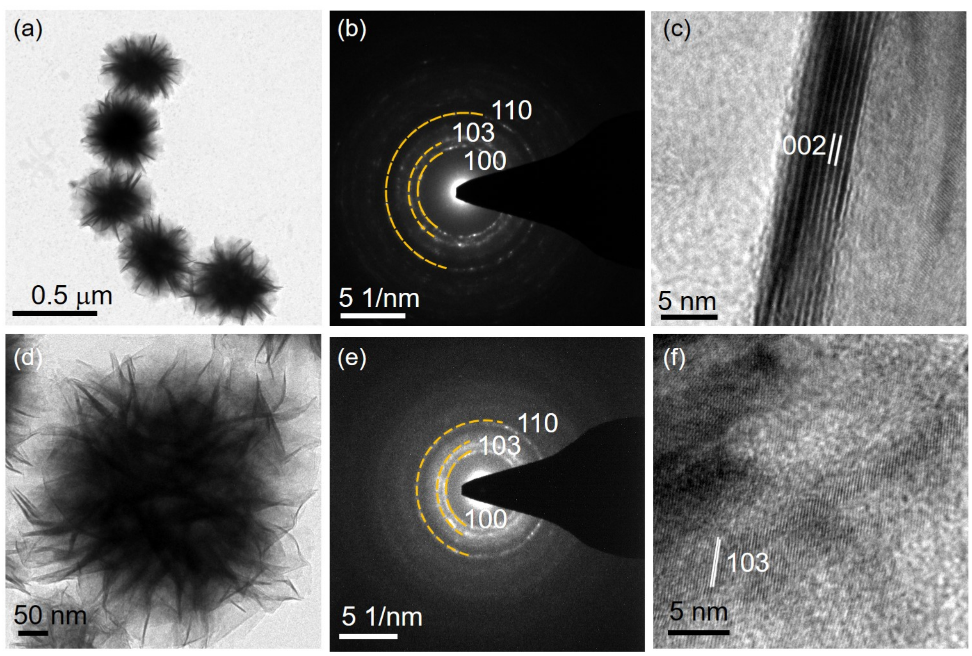

Fig. S4: Microstructural characterization of $MoSe_2$@WSe_2 hierarchical nanostructure- Low-magnification bright-field TEM micrograph showing the sheets protruding from the core, SAED pattern showing the polycrystalline nature of nanoflowers and HRTEM image of $MoSe_2$@WSe_2 of Composition A (a, b, and c) and Composition C (d, e, and f).

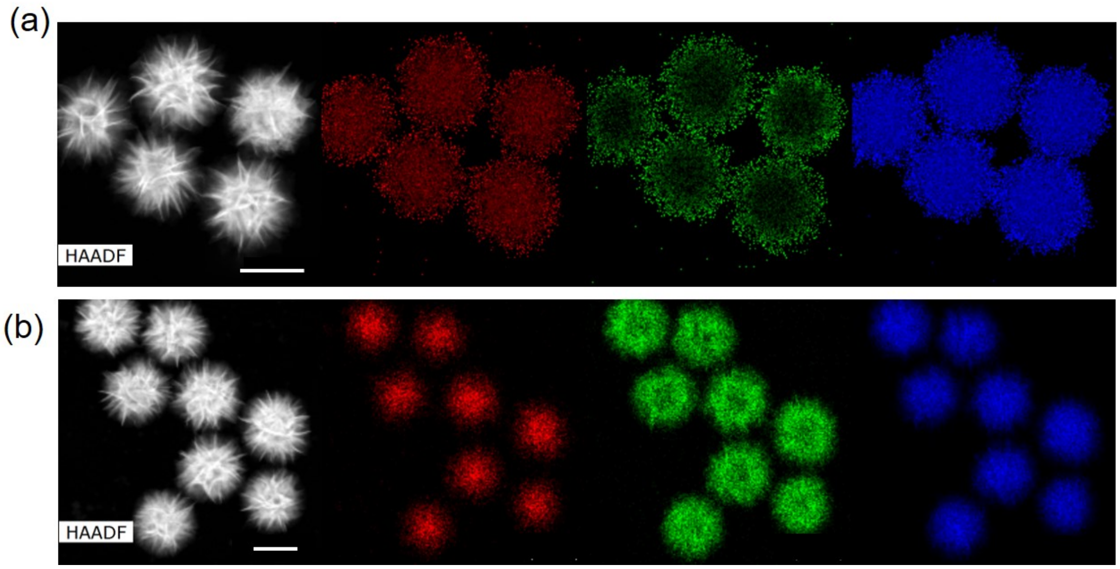

Fig. S5: HAADF-STEM image and elemental maps of Mo, W, and Se in hierarchical nanostructures of (a) Composition A and (b) Composition C. Scale bar shown in the image represent 200 nm.

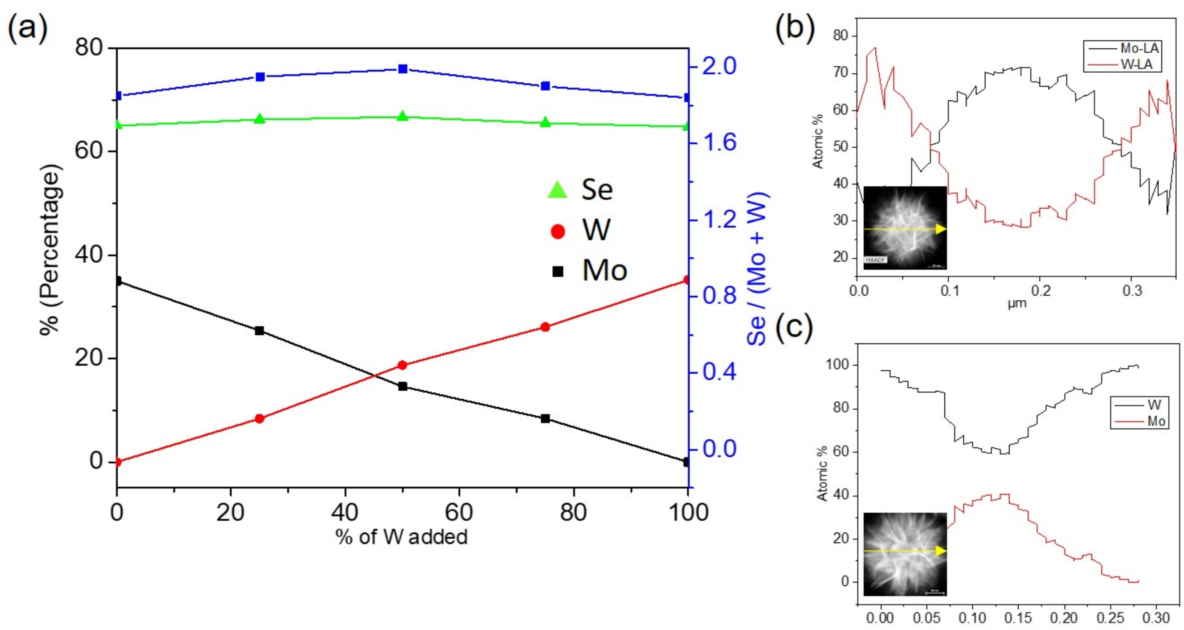

Fig. S6: (a) Overall composition of W, Mo and Se in as-synthesized nanostructures and hierarchical nanostructures. Composition profile of Mo and W along the line drawn across the nanostructures (b) Composition A, and (c) Composition C.

Table S1: Mo and W atomic % observed from STEM-EDS maps in different hierarchical nanostructures

Sample name	**Atomic% of Mo**	**Atomic% of W**
Composition A	75.1	24.9
Composition B	43.8	56.2
Composition C	24.3	75.7

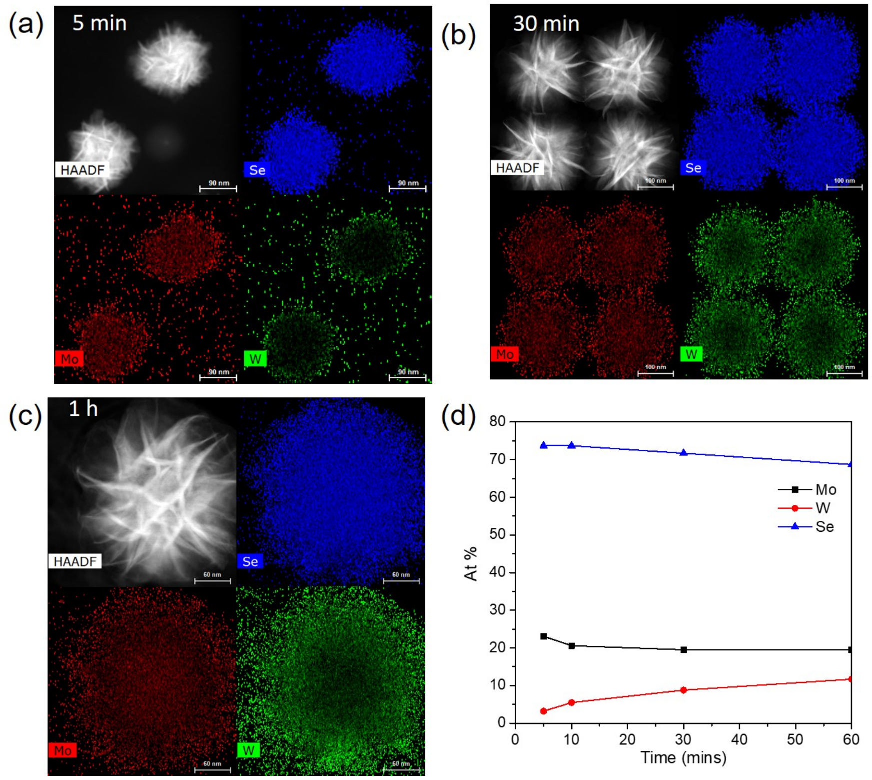

Fig. S7: HAADF-STEM image and EDS map of hierarchical nanostructure formation with 1:1 ratio of Mo:W (Composition B) after 5 mins, 30 mins and 1 h of the reaction, corresponding composition graph showing the overall composition of the product at aforementioned time interval of reaction.

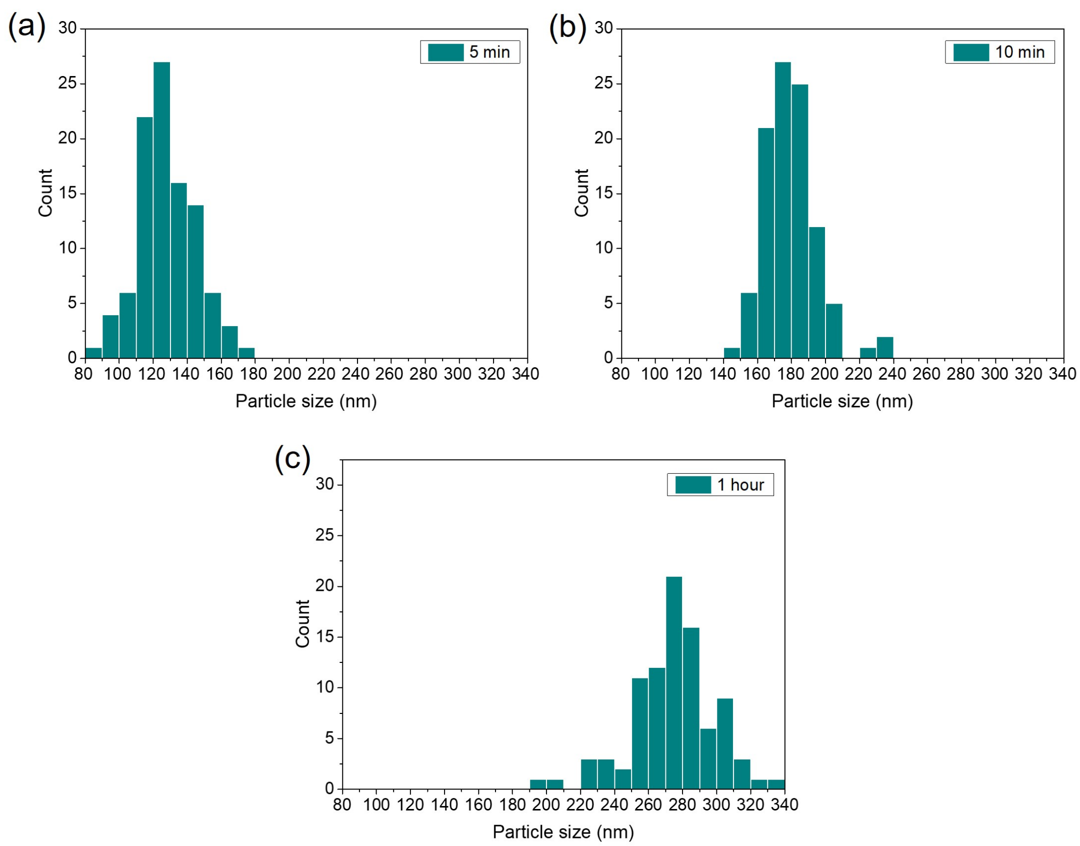

Fig. S8: Particle size distribution of time-dependent reaction product of composition B (a) 5 min; (b) 10 min, and (c) 1 h

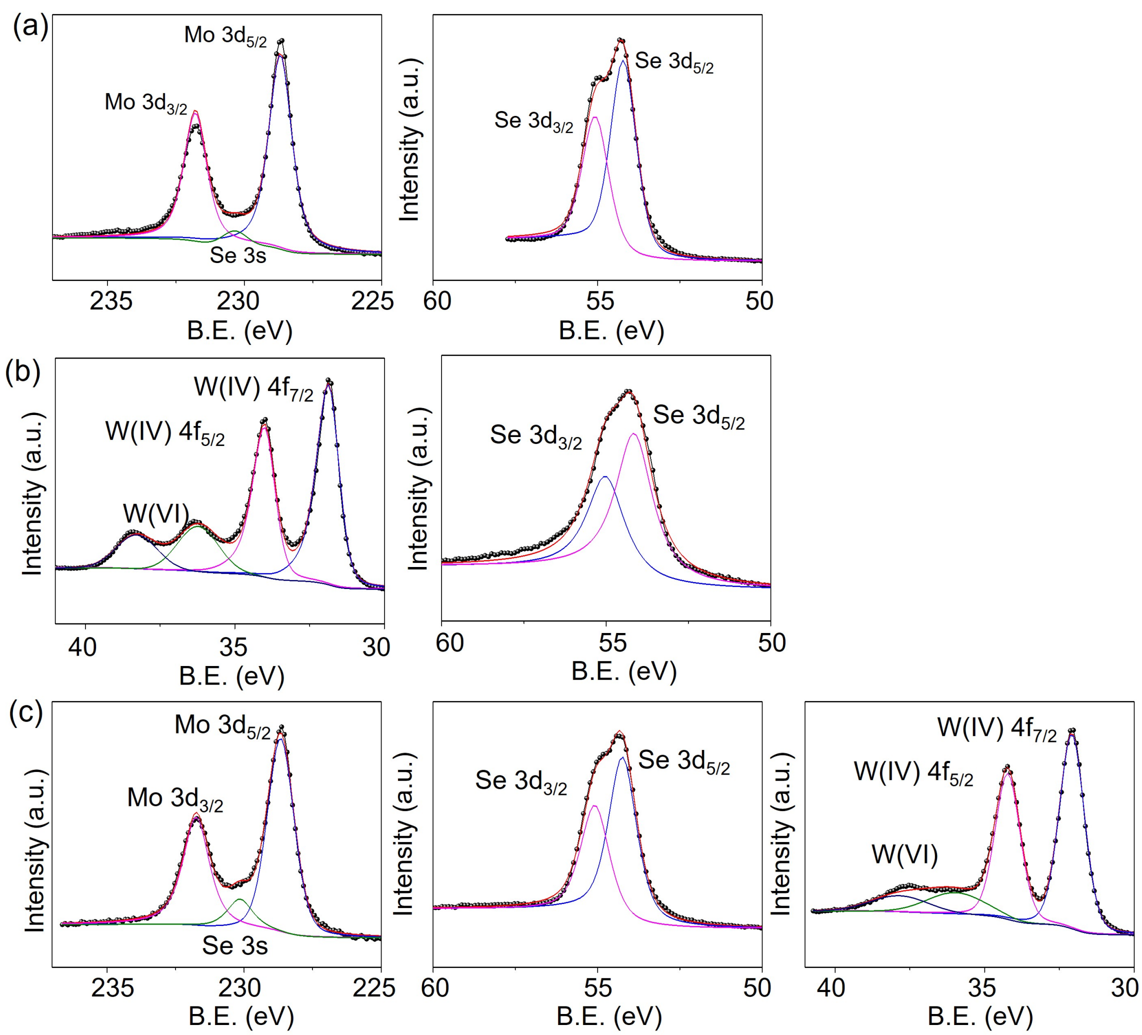

Fig. S9: HRXPS spectra of (a) $MoSe_2$; (b) WSe_2, and (c) $MoSe_2$@WSe_2 (Composition B)

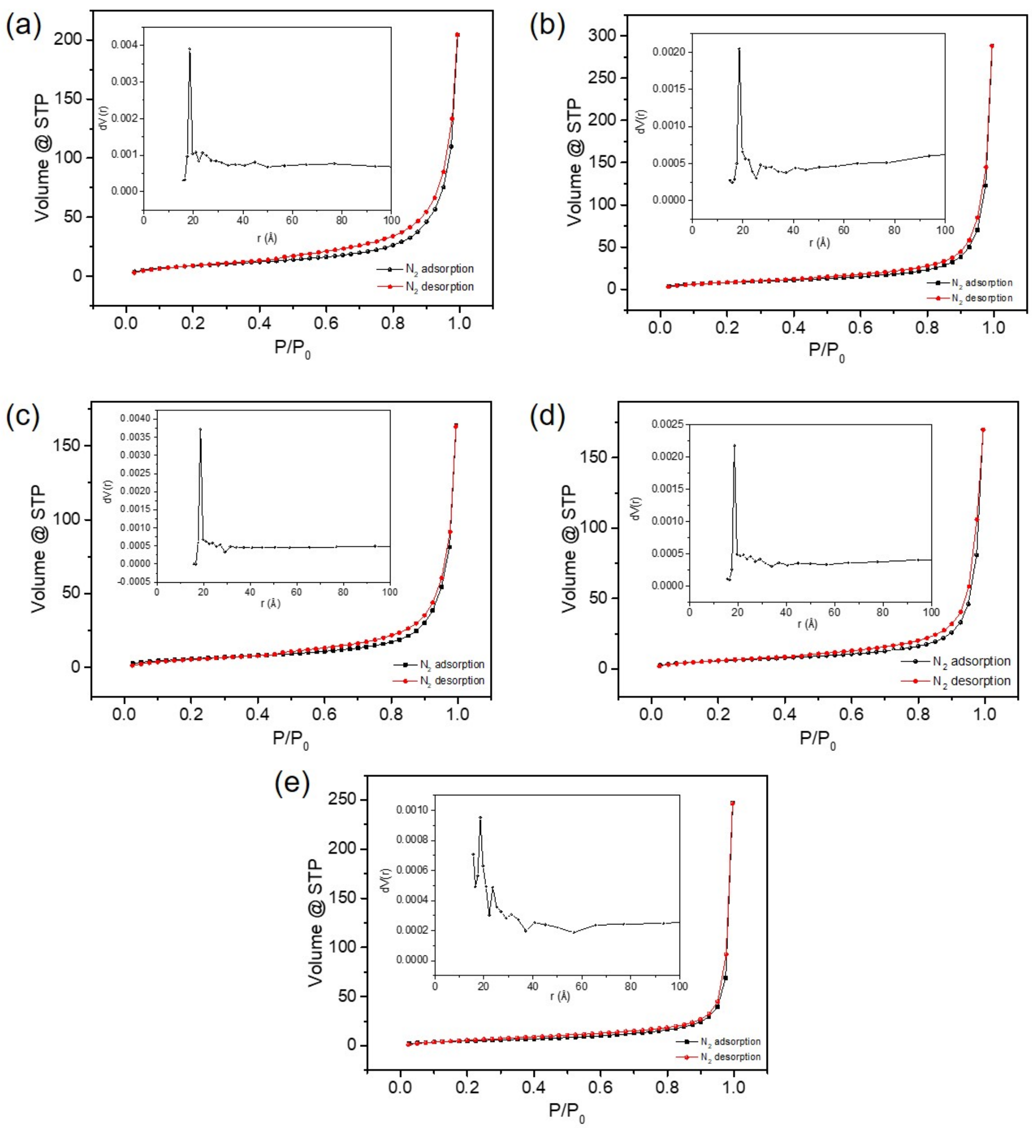

Fig. S10: N_2 adsorption-desorption isotherm (inset: average pore size distribution) of (a) $MoSe_2$; (b) Composition A; (c) Composition B; (d) Composition C, and (e) WSe_2.

Table S2: N_2 adsorption-desorption analysis using BET method.

Sample name	**Specific surface area (m^2/g)**	**Average pore size (radius, nm)**	**Average pore volume (cc/g)**
$MoSe_2$	34.384	1.8518	0.322
Composition A	31.427	1.8548	0.450
Composition B	22.973	1.8534	0.258
Composition C	22.096	1.8532	0.265
WSe_2	19.585	1.8536	0.383

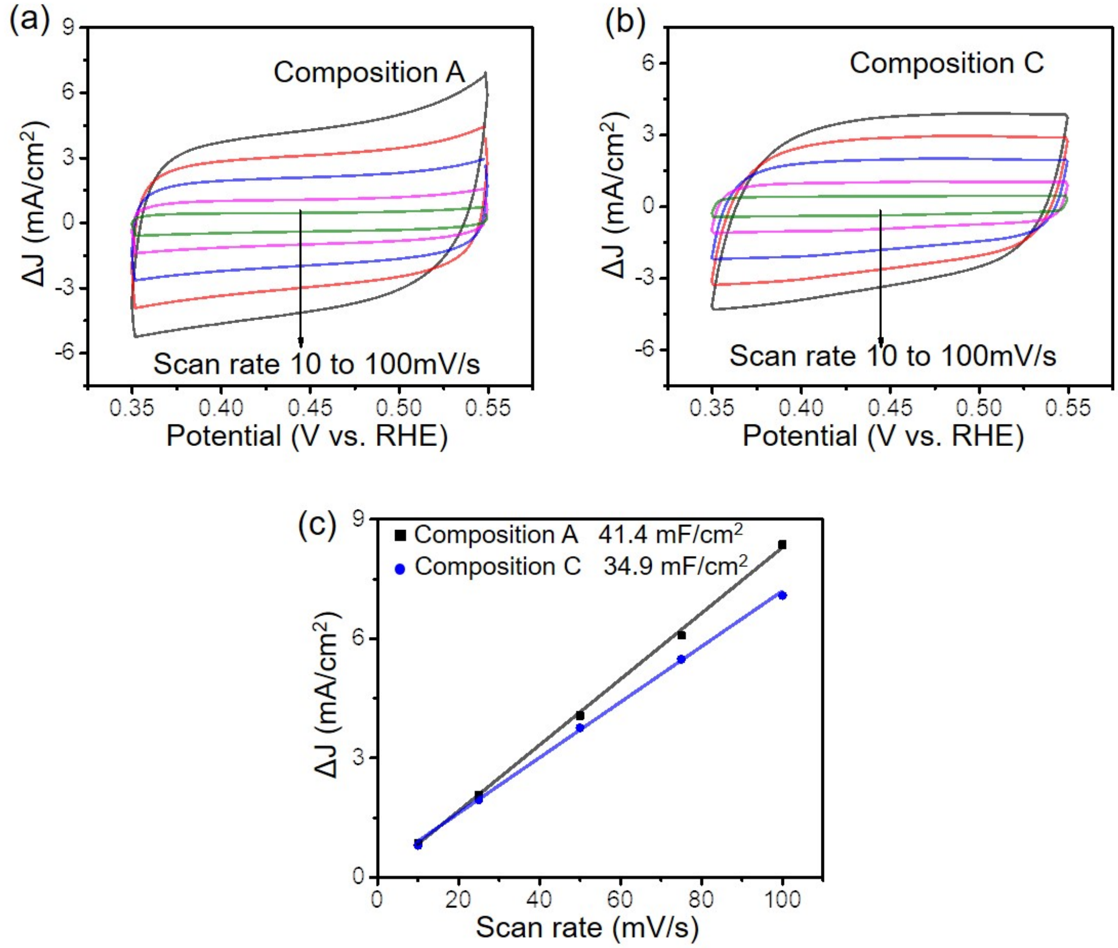

Fig. S11: CV in the faradaic region at different scan rates (10 to 100 mV/s) for (a) Composition A; (b) Composition C, and (c) corresponding C_{dl} plot

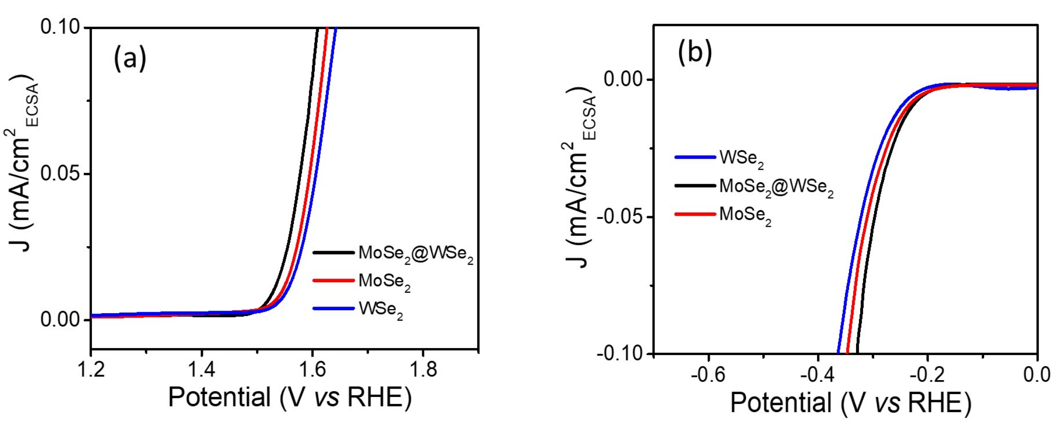

Fig. S12: ECSA normalized performance of the samples towards (a) OER and (b) HER.

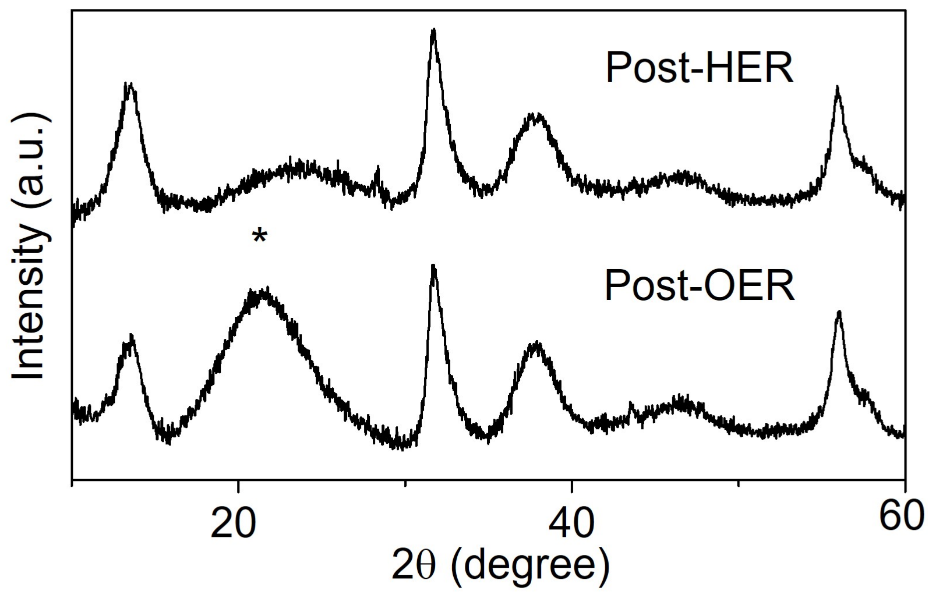

Fig. S13: XRD pattern of the catalysts after 20 h of water-splitting reaction; peak marked with * corresponds to the carbon.

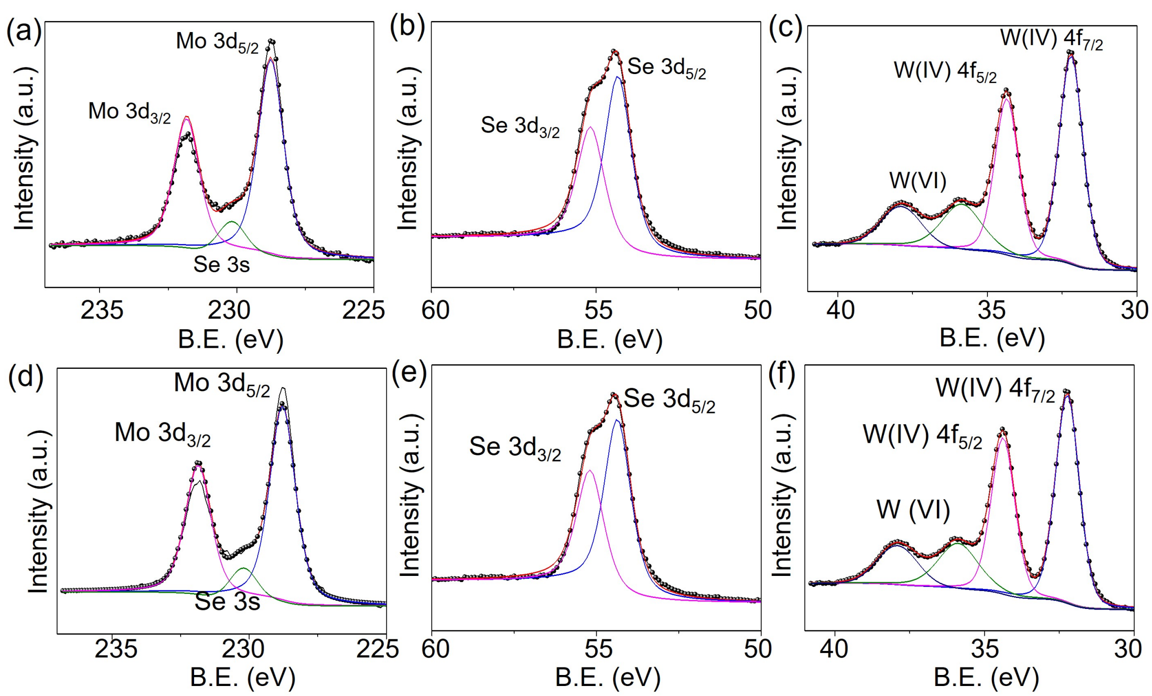

Fig. S14: (a, b, and c) HRXPS spectra of Mo 3d, Se 3d and W 4f post-OER, respectively; (d, e, and f) HRXPS spectra of Mo 3d, Se 3d and W 4f post-HER, respectively.

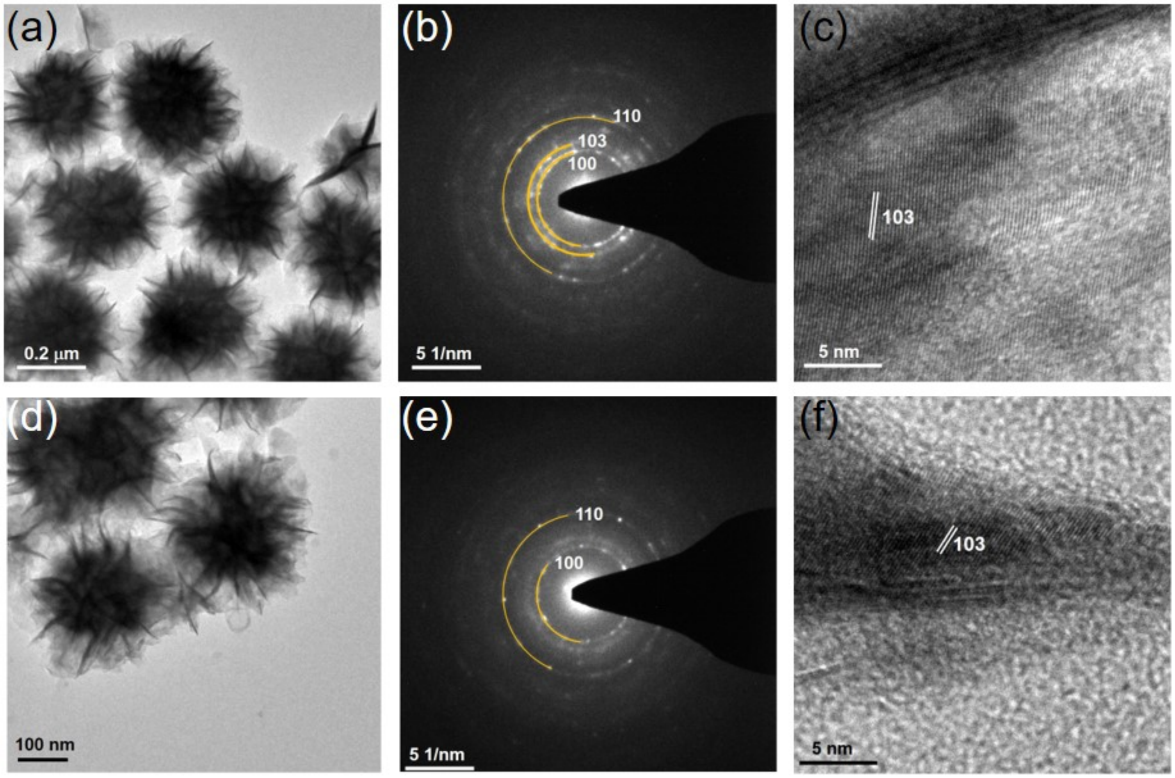

Fig. S15: Microstructural characterization of $MoSe_2$@WSe_2 (Composition B) post-electrocatalysis, (a, b, and c) low-magnification bright-field TEM micrograph, corresponding SAED pattern and HRTEM micrograph of $MoSe_2$@WSe_2 post-HER and (d, e, and f) low-magnification bright-field TEM micrograph, corresponding SAED pattern and HRTEM micrograph of $MoSe_2$@WSe_2 post-OER respectively.

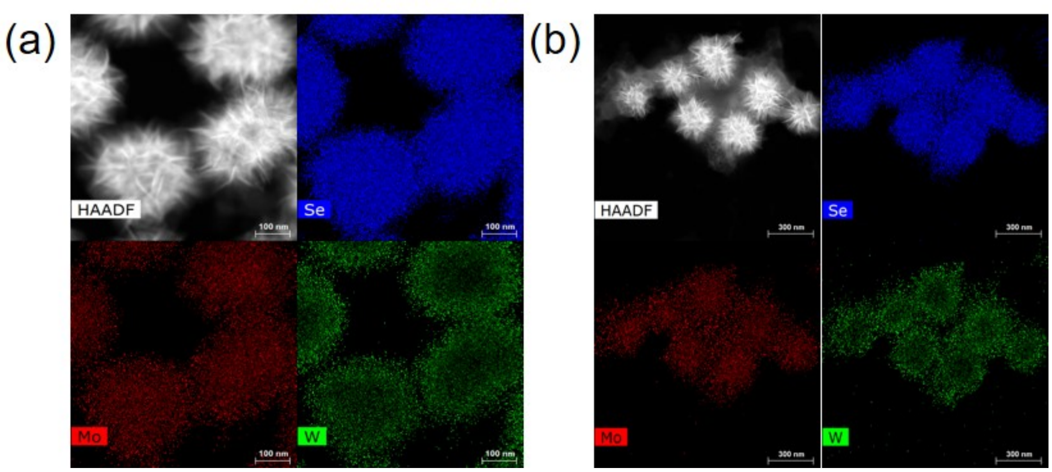

Fig. S16: STEM-EDS map showing the post-electrocatalysis elemental distribution of Mo, W and Se in $MoSe_2$@WSe_2 (Composition B) nanostructure (a) HER and (b) OER.

Table S3: Comparison of catalytic activity of $MoSe_2$@WSe_2 to other previously reported LMDs based catalyst for HER and OER in alkaline media.

Catalyst	**Electrolyte**	**Reaction: E@10 mA/cm^2 (mV)**	**Tafel slope (mV/dec)**	**Reference**
$MoSe_2$@WSe_2 (Composition B)	1.0 M KOH	HER: 231 OER: 300	HER: 87 OER: 51	This work
$MoSe_2$	1.0 M KOH	HER: 252 OER: 330	HER: 95 OER: 72	This work
WSe_2	1.0 M KOH	HER: 298 OER: 339	HER: 145 OER: 80	This work
Pristine WSe_2	0.5 M KOH	HER: 375	152	[1]
5% Ni-WSe_2	0.5 M KOH	HER: 235	120	[1]
$MoSe_2$-$CoSe_2$ NTs	1.0 M KOH	HER: 237	89	[2]
Co-WSe_2/MWNT	1.0 M KOH	HER: 241	-	[3]
MoWSe alloys	0.5 M KOH	HER: 262	101	[4]
MoS_2/$MoSe_{2-0.5}$	1.0 M KOH	HER: 235	96	[5]
$MoSe_2$	1.0 M KOH	HER: 330	135	[5]
ex-$MoSe_2$:$NiCl_2$	1.0 M KOH	HER: 273	114	[6]
$MoSe_2$	1.0 M KOH	HER: 331	137	[7]
Ni–Al-LDH–MoS_2 (NAM-2)	1.0 M KOH	OER: 310	56	[8]
$NiSe_2$	1.0 M KOH	OER: 299	63	[9]
$MoSe_2$	1.0 M KOH	OER: 386	126.2	[10]
Mo–Ni–Se@NF	1.0 M KOH	OER: 386 @ 100 mA/cm^2	44.9	[11]
0D- 2D-$CoSe_2$/$MoSe_2$	1.0 M KOH	OER: 280	86.8	[12]
$MoSe_2$	1.0 M KOH	OER: $\sim$420	130	[12]
$Ni_{0.5}Mo_{0.5}Se$	1.0 M KOH	OER: 340	-	[13]
Ag-$CoSe_2$	1.0 M KOH	OER: 320	56	[14]
Yolk–Shell Ni–Co–Se/carbon fiber paper	1.0 M KOH	OER: 300	87	[15]
$Ni_{0.85}Se$/$MoSe_2$	1.0 M KOH	OER: 340	-	[16]
$CoSe_2$@$MoSe_2$	1.0 M KOH	OER: 309	84.04	[17]
$MoSe_2$	1.0 M KOH	OER: 372	142	[17]
MoS_2-MoO_3	0.5M M H_2SO_4	HER: 250	125	[18]

Ni0.85Se/MoSe2 110/77 340/

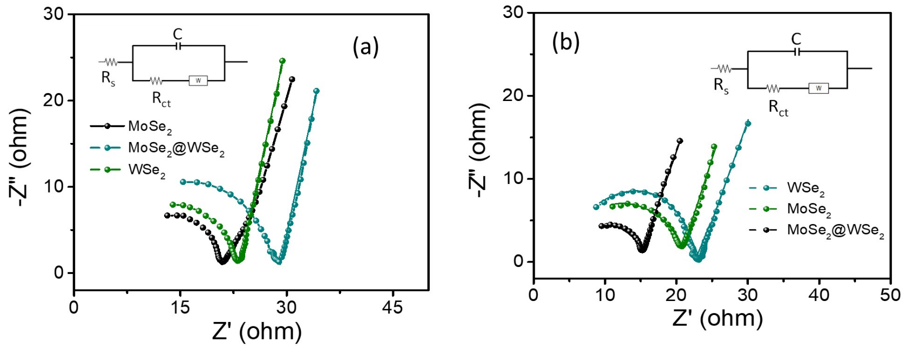

Fig. S17: Nyquist plots for the as-synthesized samples in alkaline media for (a) OER and (b) HER, inset, equivalent circuit model.

Table S4: Value of resistance (R_s + R_{ct}) as obtained from the Nyquist plot for OER and HER.

Catalyst	**R_s + R_{ct} (Ω)**	
	OER	**HER**
$MoSe_2$	23.1	20.5
WSe_2	28.8	23
$MoSe_2$@WSe_2 (Composition B)	20.7	15.2

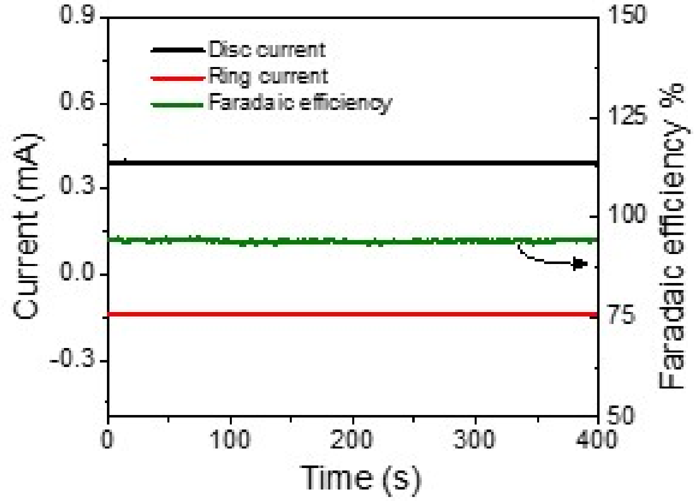

Fig. S18: Faradaic efficiency calculated using the RRDE method.

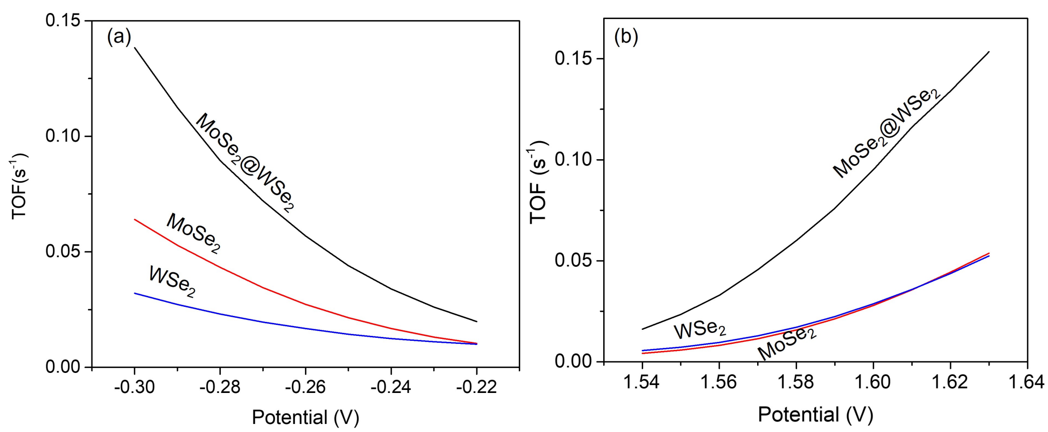

Fig. S19: TOF of as-synthesized catalysts in alkaline medium for (a)HER and (b) OER

References

[1] S.R. Kadam, A.N. Enyashin, L. Houben, R. Bar-Ziv, M. Bar-Sadan, Ni–WSe_2 nanostructures as efficient catalysts for electrochemical hydrogen evolution reaction (HER) in acidic and alkaline media, Journal of Materials Chemistry A, 8 (2020) 1403-1416.

[2] X. Wang, B. Zheng, B. Yu, B. Wang, W. Hou, W. Zhang, Y. Chen, In situ synthesis of hierarchical $MoSe_2$–$CoSe_2$ nanotubes as an efficient electrocatalyst for the hydrogen evolution reaction in both acidic and alkaline media, Journal of Materials Chemistry A, 6 (2018) 7842-7850.

[3] G. Zhang, X. Zheng, Q. Xu, J. Zhang, W. Liu, J. Chen, Carbon nanotube-induced phase and stability engineering: a strained cobalt-doped WSe_2/MWNT heterostructure for enhanced hydrogen evolution reaction, Journal of Materials Chemistry A, 6 (2018) 4793-4800.

[4] O.E. Meiron, V. Kuraganti, I. Hod, R. Bar-Ziv, M. Bar-Sadan, Improved catalytic activity of $Mo_{1x}W_xSe_2$ alloy nanoflowers promotes efficient hydrogen evolution reaction in both acidic and alkaline aqueous solutions, Nanoscale, 9 (2017) 13998-14005.

[5] Q. Zhou, G. Zhao, K. Rui, Y. Chen, X. Xu, S.X. Dou, W. Sun, Engineering additional edge sites on molybdenum dichalcogenides toward accelerated alkaline hydrogen evolution kinetics, Nanoscale, 11 (2019) 717-724.

[6] L. Najafi, S. Bellani, R. Oropesa-Nuñez, A. Ansaldo, M. Prato, A.E. Del Rio Castillo, F.J.A.E.M. Bonaccorso, Doped-$MoSe_2$ Nanoflakes/3d Metal Oxide–Hydr (Oxy) Oxides Hybrid Catalysts for pH-Universal Electrochemical Hydrogen Evolution Reaction, 8 (2018) 1801764.

[7] G. Zhao, P. Li, K. Rui, Y. Chen, S.X. Dou, W. Sun, $CoSe_2$/$MoSe_2$ Heterostructures with Enriched Water Adsorption/Dissociation Sites towards Enhanced Alkaline Hydrogen Evolution Reaction, Chemistry – A European Journal, 24 (2018) 11158-11165.

[8] M.S. Islam, M. Kim, X. Jin, S.M. Oh, N.-S. Lee, H. Kim, S.-J. Hwang, Bifunctional 2D Superlattice Electrocatalysts of Layered Double Hydroxide–Transition Metal Dichalcogenide Active for Overall Water Splitting, ACS Energy Letters, 3 (2018) 952-960.

[9] C. Cai, Y. Mi, S. Han, Q. Wang, W. Liu, X. Wu, Z. Zheng, X. Xia, L. Qiao, W. Zhou, X. Zu, Engineering ordered dendrite-like nickel selenide as electrocatalyst, Electrochimica Acta, 295 (2019) 92-98.

[10] M. Yuan, S. Dipazir, M. Wang, Y. Sun, D. Gao, Y. Bai, M. Zhang, P. Lu, H. He, X. Zhu, S. Li, Z. Liu, Z. Luo, G. Zhang, Polyoxometalate-assisted formation of CoSe/$MoSe_2$ heterostructures with enhanced oxygen evolution activity, Journal of Materials Chemistry A, 7 (2019) 3317-3326.

[11] H. Yang, Y. Huang, W.Y. Teoh, L. Jiang, W. Chen, L. Zhang, J. Yan, Molybdenum Selenide nanosheets Surrounding nickel Selenides Sub-microislands on nickel foam as high-performance bifunctional electrocatalysts for water Splitting, Electrochimica Acta, 349 (2020) 136336.

[12] L. Xia, H. Song, X. Li, X. Zhang, B. Gao, Y. Zheng, K. Huo, P.K. Chu, Hierarchical 0D2D Co/Mo Selenides as Superior Bifunctional Electrocatalysts for Overall Water Splitting, 8 (2020).

[13] K. Premnath, P. Arunachalam, M.S. Amer, J. Madhavan, A.M. Al-Mayouf, Hydrothermally synthesized nickel molybdenum selenide composites as cost-effective and efficient trifunctional electrocatalysts for water splitting reactions, International Journal of Hydrogen Energy, 44 (2019) 22796-22805.

[14] X. Zhao, H. Zhang, Y. Yan, J. Cao, X. Li, S. Zhou, Z. Peng, J. Zeng, Engineering the Electrical Conductivity of Lamellar Silver-Doped Cobalt(II) Selenide Nanobelts for Enhanced Oxygen Evolution, Angewandte Chemie International Edition, 56 (2017) 328-332.

[15] K. Ao, J. Dong, C. Fan, D. Wang, Y. Cai, D. Li, F. Huang, Q. Wei, Formation of Yolk–Shelled Nickel–Cobalt Selenide Dodecahedral Nanocages from Metal–Organic Frameworks for Efficient Hydrogen and Oxygen Evolution, ACS Sustainable Chemistry Engineering, 6 (2018) 10952-10959.

[16] H.R. Inta, S. Ghosh, A. Mondal, G. Tudu, H.V.S.R.M. Koppisetti, V. Mahalingam, $Ni_{0.85}Se/MoSe_2$ Interfacial Structure: An Efficient Electrocatalyst for Alkaline Hydrogen Evolution Reaction, ACS Appl Energy Mater. 4 (2021) 2828–2837.

[17] Z. Chen, W. Wang, S. Huang, P. Ning, Y. Wu, C. Gao, T.T. Le, J. Zai, Y. Jiang, Z. Hu, X. Qian, Well-defined $CoSe_2$@$MoSe_2$ hollow heterostructured nanocubes with enhanced dissociation kinetics for overall water splitting, Nanoscale. 12 (2020) 326–335.

[18] L. Sharma, T. Botari, C.S. Tiwary, A. Halder, Hydrogen Evolution at the In Situ MoO_3/MoS_2 Heterojunctions Created by Nonthermal O_2 Plasma Treatment, ACS Appl. Energy Mater. 2020, 3, 6, 5333–5342.